Jestr

Journal of Engineering Science and Technology Review 9 (4) (2016) 120 - 127

Research Article

JOURNAL OF
Engineering Science and Technology Review

www.jestr.org

A Novel Method for Stress Calculation Considering the Creep Behaviour of Shale Gas Reservoir

Chong Yu[1,*], Haibo Li[1], Renji Wu[1] and Yuqi Sun[2]

[1]*China State Key Laboratory of Geomechanics and Geotechnical Engineering, Institute of Rock and Soil Mechanics, Chinese Academy of Sciences, Wuhan 430071, China*
[2] *CISS Engineering Depart, Oire Prianza 12 - 78521, Bologna, Italy*

Received 12 May 2016; Accepted 2 September 2016.

Abstract

To study the creep effect on the stress field under gas–solid thermal coupling, a novel method for stress calculation considering the creep behaviour of shale gas reservoir was proposed based on the principle of least energy consumption. Then, laboratory tests and mathematical fitting methods were adopted to analyze the creep constitutive model for shale, existence states of shale gas, stress, and temperature. In addition, the nonlinear relationship among permeability coefficient, porosity, and volumetric strain was theoretically derived. Results indicated that the established creep damage model can describe not only the decay and steady creep stages, but also the accelerating creep stage. The temperature effect on the mechanical properties of the rock mass conformed to polynomial characteristics. The elastic modulus slowly decreased and the viscosity coefficient rapidly decreased with increasing temperature. The temperature effect on shale gas adsorption conformed to linear characteristics. The Langmuir volume and Langmuir pressure were inversely proportional to temperature; the deceleration of the former was faster than that of the latter. The proposed method can be used to evaluate the stress field of shale gas wells. This research provides a novel approach for refracturing and analysis of gas flow in shale gas wells.

Keywords: Shale, Creep model, Stress field, Coupling analysis

1. Introduction

China has good prospects for shale gas exploration. China Petro-Chemical Corporation has proven the presence of shale gas geological reserves of 380.598 billion m^3 in an area of 383.54 km^2 in the Jiaoshiba District of Chongqing City. This site is the world's second largest shale gas field, second only to that in North America. Thus, China is accelerating the deployment of shale gas exploration and development.

Shale gas is natural gas that accumulated in dark shale or high-carbon shale mainly in the free and adsorption states. Pore pressure affects the effective stress of a shale gas reservoir because of the free-state shale gas. Adsorption and desorption of shale gas also alter the mechanical properties of shale. Both existence states of shale gas elicit mechanical responses to shale. A shale gas reservoir is characterized by a high ground temperature, large embedded depth, low permeability, and long-term exploitation, thereby complicating stress calculation.

The output of shale gas inevitably causes variations in the initial stress and thus influences refracturing and gas flow in a shale gas well. Hence, a new method must be established for stress calculations in a shale gas reservoir.

2. State of the art

Much research has focused on analysis of stress changes in shale gas reservoirs. Basing on the pressure from refracturing treatments and the simulations of horizontal stress changes, Elbel and Mack [1] suggested that the horizontal principal stress near the wells was reversed under the combined action of the initial hydraulic fracture and the pore pressure gradients caused by production. The initiation of the refracture plane would appear normal to the initial fracture plane because of variations in local stress field. Roussel and Sharma [2] reported similar results: the stress around the production well was reoriented because of the non-uniform depletion of the reservoir. Initially, the direction of maximum horizontal stress was aligned with the initial fracture. During the production, the maximum horizontal stress decreased faster than the minimum horizontal stress because of the higher depletion in the fracture, thereby causing stress reversal in the vicinity of the fracture. Gupta et al. [3] revealed the spatial and temporal distribution of reservoir stress for two case studies of shale gas wells from ExxonMobil; their work proved that the fracturing opportunity and fracture propagation could be manipulated by injecting, shutting-in, and producing offset wells. Zhai and Abou-Sayed [4] evaluated the thermal stress and poro-elastic stress effects on stress reorientation; in some cases, temperature played an important role in stress changes. Certain research achievements on the reservoir stress change were obtained.

Under the action of temperature, stress, and shale gas, shale demonstrates certain degrees of creep characteristics.

* E-mail address: cyu@whrsm.ac.cn

This trend also changed the distribution of reservoir stress [5–7]. To date, research on this topic remains insufficient. Nevertheless, creep characteristics, creep tests, and constitutive models have been studied in other fields. Sharifzadeh et al. [8] conducted triaxial creep tests on shale specimens and numerically simulated the time-dependent behaviour of the tunnel host rock by considering the Burger-creep visco-plastic model (CVISC) embedded with FLAC3D. After 55 years of tunnel utilization, the compressive strengths of the lining concrete were not stable against stresses induced by thrust force and bending moment. Basing on the results of triaxial creep tests on clastic rock of the Xiangjiaba Hydropower Project, Zhang et al. [9] used the Burgers creep model to fit the creep curves. The Burgers model accurately described the creep behaviour of clastic rock under low stress but could not describe the accelerating creep stage under high stress. Above research achievements provide references.

To study changes in the reservoir stress under gas–solid thermal coupling, this paper proposes a new method for stress calculation considering the creep characteristics of shale in terms of energy consumption. The technology roadmap is drawn in Fig. 1. The remainder of this paper is organized as follows: Section 3 establishes a creep damage constitutive model according to the principle of least energy consumption (PLEC). Creep tests verify the validity of the model. Section 4 presents the coupling analysis that considers the temperature deterioration, shale gas state, and the dynamic changes of the permeability coefficient. Our conclusions are summarized in Section 5.

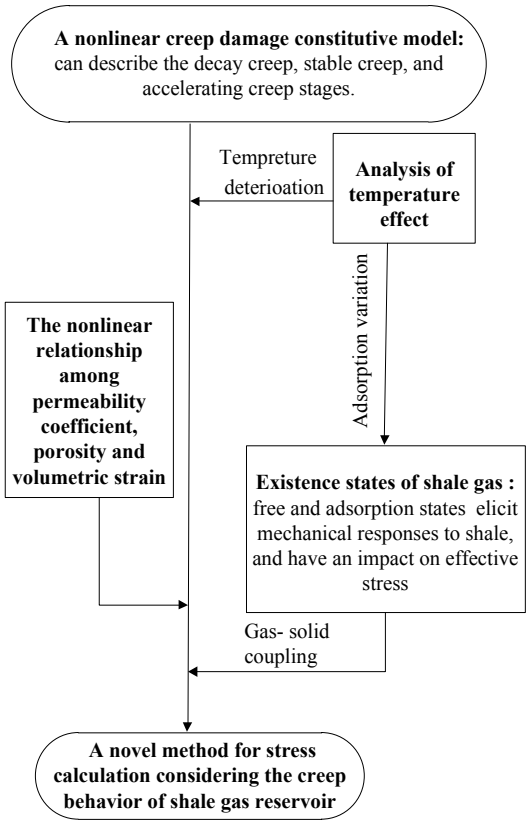

Fig. 1. Technology roadmap

3. Nonlinear creep damage constitutive model

The creep properties of rock mass are influenced by the micro-, meso-, and macro-structural planes within the rock. Damage mechanics theory is used to establish the creep damage model, which can deeply identify the deformation and failure mechanism [10–12]. Based on the Burgers model, the PLEC was applied to establish the visco-elasto-plastic constitutive model with creep damage evolution. The three-dimensional nonlinear model can describe all the creep stages (including the decay creep, stable creep, and accelerating creep stages).

3.1 Model foundation

According to the PLEC, any energy dissipation process follows the minimum energy dissipation with the corresponding constraints. "The minimum energy dissipation" is that the energy dissipation rate is the minimum value at any time during the energy dissipation process. "The corresponding constraints" refer to the control equations (such as basic equation, constitutive equation, and yield criterion) and their respective definite conditions, which should be met by the physical quantities in the expression of the energy dissipation rate. The damage evolution of the rock mass is suitable for the PLEC because this process essentially involves energy dissipation.

Before energy dissipation, the constitutive equation can be expressed as:

$$\begin{cases} \varepsilon_1' = \dfrac{1}{E}[\sigma_1' - \mu(\sigma_2' + \sigma_3')] \\ \varepsilon_2' = \dfrac{1}{E}[\sigma_2' - \mu(\sigma_1' + \sigma_3')] \\ \varepsilon_3' = \dfrac{1}{E}[\sigma_3' - \mu(\sigma_1' + \sigma_2')] \end{cases} \tag{1}$$

where E and μ are the elastic modulus and Poisson ratio before energy dissipation, respectively. σ_i' and ε_i' (i = 1,2,3) are the effective principal stress and effective principal strain, respectively.

For the energy dissipation in the accelerating creep stage, the damage variable is defined as:

$$D_a(t_a) = 1 - \psi(t_a)/\psi_0 \tag{2}$$

where t_a is the damage time; $D_a(t_a)$ is the damage variable, which ranges from 0 to 1; $\psi(t_a)$ is the material parameter. When an elastic modulus is represented, Eq. (2) is converted to:

$$D_a(t) = 1 - E(t_a)/E \tag{3}$$

According to the strain equivalence principle, the constitutive equation for isotropic damage is:

$$\begin{cases} \varepsilon_1'(t_a) = \dfrac{1}{E[1-D_a(t_a)]}[\sigma_1' - \mu(\sigma_2' + \sigma_3')] \\ \varepsilon_2'(t_a) = \dfrac{1}{E[1-D_a(t_a)]}[\sigma_2' - \mu(\sigma_1' + \sigma_3')] \\ \varepsilon_3'(t_a) = \dfrac{1}{E[1-D_a(t_a)]}[\sigma_3' - \mu(\sigma_1' + \sigma_2')] \end{cases} \tag{4}$$

The energy dissipation rate of a small unit volume is:

$$\varphi(t_a) = \sigma_i' \dot{\varepsilon}_i'(t_a) \quad (i = 1,2,3) \tag{5}$$

In the formula, $\dot{\varepsilon}_i'(t_a)$ are the effective principal strain rates. By substituting Eq. (4) into Eq. (5), we obtain:

$$\varphi(t_a) = -\frac{D_a(t_a)}{[1-D_a(t_a)]^2 E}\begin{bmatrix} \sigma_1'^2 + \sigma_2'^2 + \sigma_3'^2 - \\ 2\mu(\sigma_1'\sigma_2' + \sigma_2'\sigma_3' + \sigma_1'\sigma_3') \end{bmatrix} \tag{6}$$

The Hoek–Brown yield criterion [13] is chosen as the constraint condition:

$$F = \sigma_1' - \sigma_3' - \sigma_{ci}(m_b \frac{\sigma_3'}{\sigma_{ci}} + s)^{\alpha} = 0 \tag{7}$$

where m_b, s, and a are Hoek–Brown parameters. The value of these parameters can be calculated according to literature [14].

Based on the PLEC, the stationary value of Eq. (6) is obtained under the conditions of Eq. (7):

$$\frac{\partial[\varphi(t_a) + \lambda F]}{\partial \sigma_i} = 0 \tag{8}$$

By rearranging Eq. (8), the damage variable is defined:

$$D_a(t_a) = 1 - \exp\left\{\frac{am_b\lambda t_a}{2\varepsilon_V}(m_b \frac{\sigma_3'}{\sigma_{ci}} + s)^{a-1} + C\right\} \tag{9}$$

In the formula, ε_V is the volumetric strain; λ and C are parameters associated with lithology, which are obtained from the curve fitting of the creep test. The damage variable includes the damage time, stress level, and strain. Therefore, this variable is more comprehensive and reasonable.

When rock does not yield (F < 0), the Burgers model is used to describe the decay and steady creep stages. When the rock meets the yield condition, and into the accelerating creep stage (F ⩾ 0), the damage time period starts, and the damage variable weakens the parameters. The modified Burgers model was established to describe the accelerating creep stage. The constitutive model of nonlinear creep damage is expressed as Eq. (10). In this formula, σ_m' is the effective volumetric stress tensor; S_{ij}' is the effective deviatoric stress tensor; K and G are the bulk and shear modulus, respectively; η_K and G_k are the viscosity coefficient and shear modulus, respectively, of the Kelvin body; η_M is the viscosity coefficient of the Maxwell body.

$$\varepsilon_{ij}'(t) = \begin{cases} (\dfrac{\sigma_m'}{3K}\delta_{ij} + \dfrac{s_{ij}'}{2G}) + \dfrac{s_{ij}'}{2G_k}\left[1 - \exp(-\dfrac{G_K}{\eta_K}t)\right] + \dfrac{s_{ij}'}{2\eta_M}t & (F < 0) \\ (\dfrac{\sigma_m'}{3K(1-D_a(t_a))}\delta_{ij} + \dfrac{s_{ij}'}{2G(1-D_a(t_a))}) + \dfrac{s_{ij}'}{2\eta_M(1-D_a(t_a))}t & \\ + \dfrac{s_{ij}'}{2G_k(1-D_a(t_a))}\left[1 - \exp(-\dfrac{G_K}{\eta_K}t)\right] & (F \geq 0, \\ & 0 \leq D_a \leq 1) \end{cases} \tag{10}$$

3.2 Model validation

The laboratory creep test [15, 16] is employed to obtain the model parameters and determine the validity of the nonlinear creep damage constitutive model. Each cylindrical sample has a diameter of 50 mm and a height of 100 mm (Fig. 2).

Fig. 2. Shale sample

Creep tests were conducted on a rock triaxial testing system (Fig. 3), which can perform uniaxial and triaxial compression creep tests and describe the complete stress–strain curve. This system can provide a maximum lateral pressure of 100 MPa, and a maximum axial force of 2000 KN.

Fig. 3. Rock triaxial testing system

Under the triaxial compression tests: $\sigma_2' = \sigma_3'$, $\sigma_m' = \frac{1}{3}(\sigma_1' + 2\sigma_3')$, and $s_{11}' = \sigma_1' - \sigma_m' = \frac{2}{3}(\sigma_1' - \sigma_3')$. Thus, from Eq. (10), the axial creep equation is:

$$\varepsilon_{11}'(t) = \begin{cases} \dfrac{\sigma_1' + 2\sigma_3'}{9K} + \dfrac{\sigma_1' - \sigma_3'}{3G} + \dfrac{\sigma_1' - \sigma_3'}{3G_k}\left[1 - \exp(-\dfrac{G_K}{\eta_K}t)\right] + \dfrac{\sigma_1' - \sigma_3'}{3\eta_{\mathrm{M}}}t & (\mathrm{F} < 0) \\ \dfrac{\sigma_1' + 2\sigma_3'}{9K(1 - D_a(t_a))} + \dfrac{\sigma_1' - \sigma_3'}{3G(1 - D_a(t_a))} + \dfrac{\sigma_1' - \sigma_3'}{3\eta_{\mathrm{M}}(1 - D_a(t_a))}t & (\mathrm{F} \geq 0, \\ + \dfrac{\sigma_1' - \sigma_3'}{3G_k(1 - D_a(t_a))}\left[1 - \exp(-\dfrac{G_K}{\eta_K}t)\right] & 0 \leq D_a \leq 1) \end{cases} \tag{11}$$

If $\sigma_2' = \sigma_3' = 0$ MPa, then the creep test is uniaxial. Eq. (11) can be simplified as:

$$\varepsilon_{11}'(t) = \begin{cases} \dfrac{\sigma_1'}{9K} + \dfrac{\sigma_1'}{3G} + \dfrac{\sigma_1'}{3G_k}\left[1 - \exp(-\dfrac{G_K}{\eta_K}t)\right] + \dfrac{\sigma_1'}{3\eta_{\mathrm{M}}}t & (\mathrm{F} < 0) \\ \dfrac{\sigma_1'}{9K(1 - D_a(t_a))} + \dfrac{\sigma_1'}{3G(1 - D_a(t_a))} + \dfrac{\sigma_1'}{3\eta_{\mathrm{M}}(1 - D_a(t_a))}t & (\mathrm{F} \geq 0, \\ + \dfrac{\sigma_1'}{3G_k(1 - D_a(t_a))}\left[1 - \exp(-\dfrac{G_K}{\eta_K}t)\right] & 0 \leq D_a \leq 1) \end{cases} \tag{12}$$

The model parameters of five samples are determined by applying the least squares fitting method with Matlab, and the results are listed in Table 1. Fig. 4 presents the creep curves of shale. In Figs. 4(a)–4(d), the sample is always at low stress levels, the creep strain rate approaches 0, and the Burgers model provides a better fit to the creep data. The sample is not damaged after the creep test, and the creep characteristics are not obvious [Fig. 5(a)]. In Fig. 4(e), the rock sample reaches the yield state at high stress levels. The absolute error of fitting axial strain is approximately 14% based on the Burgers model after 60 h of creep test. By contrast, the absolute error is only 3% according to the creep damage model. The nonlinear creep damage model can describe the accelerating stage after rock into the yield state, thereby compensating for the deficiency of the Burgers model. In addition, sample has more obvious fracture planes under high pressure. The angle between the main fracture plane and the maximum principal stress is approximately 60°–70°, and the fracture surfaces are smooth [Fig. 5(b)].

Table 1. Creep model parameters

σ_1' (MPa)	σ_3' (MPa)	F (MPa)	K (GPa)	G (GPa)	G_k (GPa)	η_K (GPa·h)	η_M (GPa·h)	λ	C
15	0	-31.55	37.996	9.936	77.933	347.414	98998.445		
20	0	-26.55	37.978	9.918	81.26	374.579	98992.150		
25	0	-21.55	37.987	9.928	84.49	431.19	98992.163		
30	0	-16.55	38.000	9.941	82.841	454.697	98992.181		
200	50	22.99	32.864	11.164	20.787	3724.943	99590.070	-0.0075	0.1053

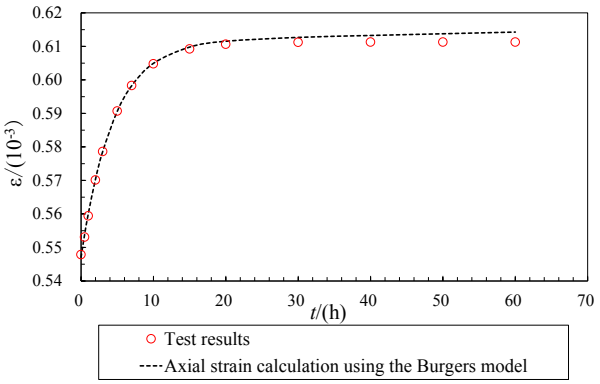

(a) σ_1 = 15 MPa, σ_3 = 0 MPa

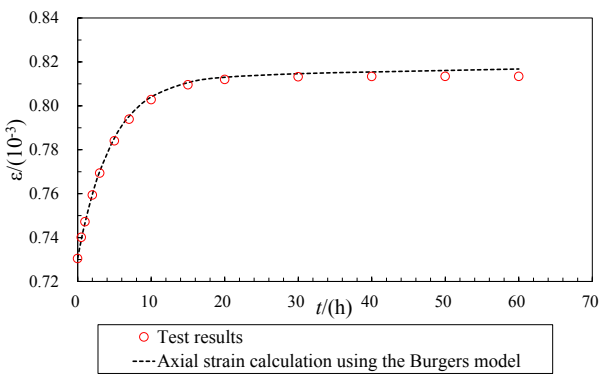

(b) σ_1 = 20 MPa, σ_3 = 0 MPa

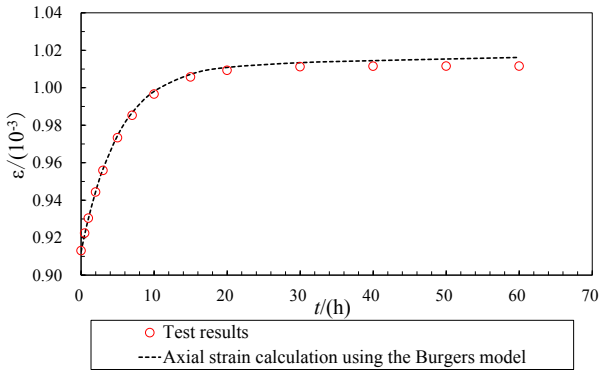

(c) σ_1 = 25 MPa, σ_3 = 0 MPa

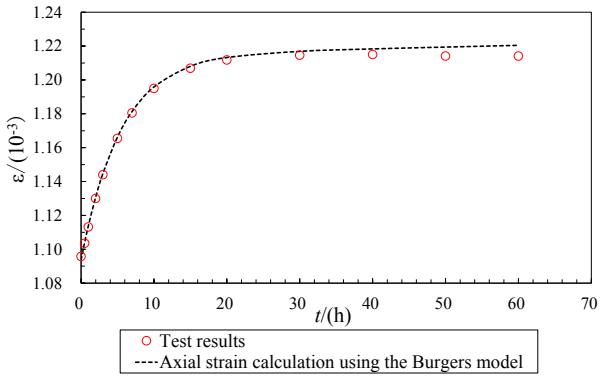

(d) σ_1 = 30 MPa, σ_3 = 0 MPa

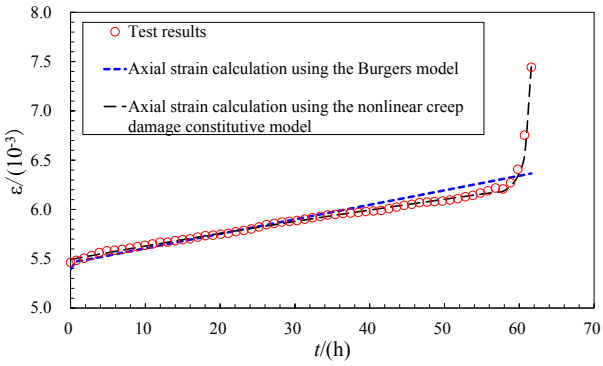

(e) σ_1 = 200 MPa, σ_3 = 50 Mpa

Fig. 4. Creep curves of shale

(a) Low stress levels

(b) High stress levels

Fig. 5. Creep curves of shale

4. Multi-field coupling analysis

4.1 Temperature effects

The ground temperature is approximately 85 °C and 120 °C at depths of 2400 and 3500 m, respectively, in the China's first national shale gas demonstration zone (Jiaoshiba shale gas production area). The effects of the temperature field on the shale gas reservoir are composed of two main aspects: (1) effects on the mechanical properties of the rock mass; (2) changes in the adsorption capacity of shale gas.

Similar to the rheological process of granite and sandstone, the microstructure changes because of the temperature; consequently, the macro mechanical properties are accordingly changed [17]. To describe this characteristic, the elastic modulus degradation factor ($D_{TE}(T)$) and the viscosity coefficient degradation factor ($D_{T\eta}(T)$) are defined as:

$$D_{TE}(T) = 1 - E(T)/E_0 \tag{13}$$

$$D_{T\eta}(T) = 1 - \eta(T)/\eta_0 \tag{14}$$

where E_0 and η_0 are the elastic modulus and viscosity coefficient, respectively, at room temperature (20 °C); $E(T)$ and $\eta(T)$ are the elastic modulus and viscosity coefficient, respectively, at the given temperature T (°C). Based on experimental data in literature [17], the fitting polynomials for $D_{TE}(T)$ and $D_{T\eta}(T)$ are:

$$D_{TE}(T) = -5\times10^{-7}T^2 + 0.0009T - 0.015 \tag{15}$$

$$D_{T\eta}(T) = -3\times10^{-6}T^2 + 0.0032T - 0.06 \tag{16}$$

When the temperature is 20 °C, $D_{TE}(T)$ and $D_{T\eta}(T)$ are almost 0; specifically, the mechanical parameters are not reduced. When the temperature is 85 °C, $D_{TE}(T) = 0.06$ and $D_{T\eta}(T) = 0.19$; that is, the elastic modulus and viscosity coefficient are reduced by 6% and 19%, respectively. As the

temperature increases to 120 °C, $D_{TE}(T) = 0.09$ and $D_{T\eta}(T) = 0.28$; thus, the elastic modulus and viscosity coefficient are reduced by 9% and 28%. The elastic modulus slowly decreases as the temperature increases, whereas the viscosity coefficient decreases rapidly with increasing temperature.

According to the isothermal adsorption equation, temperature increases at constant pressure, thereby reducing the adsorbed gas. Temperature affects the adsorption capacity of shale gas. The Langmuir equation is widely used for shale gas yield analysis in North America:

$$V = V_L p/(p_L + p) = abp/(1+bp) \quad (17)$$

where V is the adsorption capacity, m^3/t; p is the gas pressure in the reservoir, MPa; a and b are the adsorption constants under the given temperature and pressure; V_L is the Langmuir volume, m^3/t, which indicates the maximum adsorption volume; p_L is the Langmuir pressure, MPa, which is the corresponding pressure when the adsorption volume is $V_L/2$.

The test results of isothermal adsorption in 4 shale samples from the Jiaoshiba shale gas production area are listed in Table 2.

Tab. 2. Test results of isothermal adsorption [18]

Test temperature (°C)	V_L (m^3/t)		p_L (MPa)	
	Range	Average	Range	Average
30	2.03–3.36	2.71	2.14–3.31	2.54
40	1.98–3.18	2.62	2.12–3.25	2.48
50	1.94–3.05	2.52	2.08–3.14	2.41
60	1.83–2.92	2.44	2.01–3.09	2.35

Based on above test results, the linear fitting equations between V_L, p_L, and temperature are described by Eqs. (18) and (19). The results of the tests are shown in Fig. 6.

$$V_L = -0.0091T + 2.982 \quad (18)$$

$$p_L = -0.0064T + 2.733 \quad (19)$$

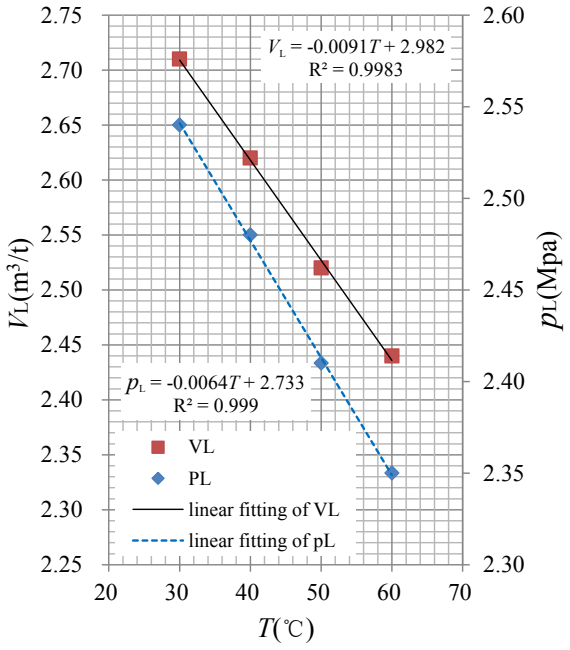

Fig. 6. Relation diagram of V_L, p_L, and temperature

From Fig. 6, the Langmuir volume and Langmuir pressure are inversely proportional to the temperature; the deceleration of the former is faster than that of the latter. When the test temperature is 85 °C, V_L = 2.21 m^3/t and p_L = 2.19 MPa. At a test temperature of 120 °C, V_L = 1.97 m^3/t and p_L = 1.89 MPa.

4.2 Existence states of shale gas

Shale gas has three existence states: the adsorbed state on the surface of organic matters and clay particles; the free state in natural fractures and pores; the dissolved state in kerogens and asphaltenes. The third state can be neglected given the limited amount of reservoir water and dissolved gas.

The swelling stress of adsorption is produced in coal bed, shale, and other porous media. The adsorbed shale gas is estimated to account for 20% to 85% of the total shale gas. Based on principles of surface physical chemistry, the swelling stress can be calculated from the results of the present study by the following formula [19]:

$$\sigma_{sw} = \frac{2a\rho R_o K(1-2\upsilon)\ln(1+bp)}{3V_m} \quad (20)$$

where ρ is the density of shale; K is the absolute temperature; V_m is the molar volume of the gas (22.4×10^{-3} m^3/mol); R_0 is molar gas constant, (8.3143 J/mol/K); the adsorption constants (a and b) can be determined by Eq. (17).

By considering adsorbed and free states of shale gas, the effective stress in the shale reservoir is:

$$\sigma'_{ij} = \sigma_{ij} - \delta_{ij}\left[\varphi p + \frac{2a\rho R_o K(1-2\upsilon)\ln(1+bp)}{3V_m}\right] \quad (21)$$

where σ'_{ij} is the effective stress tensor; σ_{ij} is the total stress tensor; δ_{ij} is the Kronecker symbol; φ is the porosity of shale.

4.3 Nonlinear relationship among permeability coefficient, porosity, and volume strain

Shale gas exploitation is a typical gas–solid coupling problem. The permeability coefficient changes with the strain of the rock mass and influences the stress field. Therefore, the nonlinear relationship of the permeability coefficient, porosity, and volume strain should be analyzed to establish the stress calculation of shale gas reservoirs.

A theoretical derivation is adopted according to the definition of porosity:

$$\varphi_0 = 1 - \frac{V_s}{V} \tag{22}$$

In the formula, φ_0 is the initial porosity, V_s represents the volume of the solid skeleton in a porous medium, and V indicates the total volume of the porous medium. Under disturbance stress, the porosity becomes:

$$\varphi = 1 - \frac{V_s + \Delta V_s}{V + \Delta V} = 1 - \frac{V_s(1 + \frac{\Delta V_s}{V_s})}{V(1 + \frac{\Delta V}{V})} \tag{23}$$

In the formula, ΔV_s and ΔV are the volume variations of the skeleton volume and total volume, respectively. Substituting Eq. (22) and volume strain ($\varepsilon_v = \frac{\Delta V}{V}$) into Eq. (23) yields:

$$\varphi = 1 - \frac{(1 - \varphi_0)(1 + \frac{\Delta V_s}{V_s})}{1 + \varepsilon_v} \tag{24}$$

By assuming that the gas stiffness is much less than the rock stiffness, ΔV_s can be neglected because it is much lower than ΔV ; thus, the equation above can be simplified to:

$$\varphi = 1 - \frac{(1 - \varphi_0)}{1 + \varepsilon_v} \tag{25}$$

Kozeny and Carman [20] proposed a relation between the permeability coefficient and porosity for porous media:

$$k = \frac{\varphi^3}{5(1-\varphi)^2}(\frac{D_{eff}}{6})^2 \tag{26}$$

In the formula, D_{eff} is the average value of the effective particle size, which does not change when the volume of rock skeleton does not change; k is the permeability coefficient, as compared with the initial permeability coefficient (k_0):

$$\frac{k}{k_0} = \frac{\varphi^3(1-\varphi_0)^2}{\varphi_0^3(1-\varphi)^2} \tag{27}$$

By substituting Eq. (25) into Eq. (27), the nonlinear relation of the permeability coefficient, porosity, and volume strain is determined:

$$k = \frac{k_0}{1 + \varepsilon_v}(1 + \frac{\varepsilon_v}{\varphi_0})^3 \tag{28}$$

5. Conclusions

Under the action of temperature, stress, and shale gas, shale demonstrates certain creep characteristics. To analyze the effect of creep characteristics on reservoir stress, this study combined theoretical derivations and laboratory tests to study the creep constitutive model and a novel method for stress calculation. The following conclusions were drawn:

(1) The established creep damage model can describe not only decay and steady creep stages but also accelerating creep stage to compensate for the deficiency of the Burgers model. Under a confining pressure of 50 MPa, an axial compression of 200 MPa, and a creep time of 60 h, the absolute error of the fitting axial strain is approximately 14% according to the Burgers model; whereas the absolute error is only 3% with the creep damage model.

(2) The elastic modulus and viscosity coefficient decrease as the temperature increases, although the deceleration of the viscosity coefficient is faster than that of the elastic modulus. When the temperature rises from 20 °C to 85 °C, the elastic modulus is reduced by 6%, whereas the viscosity coefficient is reduced by 19%. When the temperature rises to 120 °C, the elastic modulus and the viscosity coefficient are reduced by 9% and 28%, respectively. Based on the test results of the isothermal adsorption of shale samples from the Jiaoshiba shale gas production area, the adsorption capacity of shale linearly decreased with increasing temperature. The deceleration of the Langmuir pressure is slower than that of the Langmuir volume. When the temperature increases from 30 °C to 85 °C, the Langmuir volume decreases from 2.71 m^3/t to 2.21 m^3/t, whereas the Langmuir pressure decreases from 2.54 MPa to 2.19 MPa. When the temperature reaches 120 °C, the Langmuir volume is 1.97 m^3/t and the Langmuir pressure is 1.89 MPa.

(3) Given the basic assumption that gas stiffness is much less than the rock stiffness, the relation between the permeability coefficient and the volume strain is deduced to be in accordance with a power function by neglecting the volume variation values of skeleton volume. The relation is also affected by the initial permeability coefficient and initial porosity.

This paper presents a stress calculation method that considers the creep characteristics of shale and reservoir conditions. The work has some practical value for the large-scale and long-term exploitation of shale gas in China. Further work includes the writing of the corresponding calculation program or the secondary development on existing commercial software to provide a numerical calculation program based on the established method of stress calculation for shale gas reservoir.

Acknowledgements

This work was supported by the Strategic Priority Research Program of the Chinese Academy of Sciences (Grant Nos. XDB10030202) and the National Natural Science Foundation of China (Grant Nos. 41302239).

References

1. Elbel J. L., Mack M. G., "Refracturing: Observations and theories". *SPE Production Operations Symposium*, Oktahoma City, USA: SPE, 1993, pp.1-11. doi: http://dx.doi.org/10.2118/25464-MS.
2. Roussel N. P., Sharma M. M., "Role of stress reorientation in the Success of refracture treatments in tight gas sands". *SPE Production & Operations*, 27(4), 2012, pp.346-355.
3. Gupta J., Zielonka M., Albert R. A., El-Rabaa A. M., Burnham H.A., Choi N. H., "Integrated methodology for optimizing development of unconventional gas resources ". *SPE Hydraulic Fracturing Technology Conference*, The Woodlands, USA: SPE, 2012, pp.1-16. doi: http://dx.doi.org/10.2118/152224-MS.
4. Zhai Z., Abou-sayed A., "Thermal-poro plastic stress effect on stress reorientation in production and injection wells". *Brasil Offshore*, Macaé, Brazil: SPE, 2011, pp.1-15. doi: http://dx.doi.org/10.2118/140948-MS.
5. LI Y. W., Ghassemi, A., "Creep behavior of barnett, haynesville, and marcellus shale". *46th U.S. Rock Mechanics/Geomechanics Symposium*, Chicago, USA: ARMA, 2012, pp.1-7.
6. Sone H., Zoback M. D., "Strength, creep and frictional properties of gas shale reservoir rocks". *44th U.S. Rock Mechanics Symposium and 5th U.S.-Canada Rock Mechanics Symposium*, Salt Lake City, USA: ARMA, 2010, pp.1-5.
7. Sone H., Zoback M. D., "Visco-plastic properties of shale gas reservoir rocks". *45th U.S. Rock Mechanics/Geomechanics Symposium*, San Francisco, USA: ARMA, 2011, pp.1-7.
8. Shairfzadeh M., Tarifard A., Moridi M. A., "Time-dependent behavior of tunnel lining in weak rock mass based on displacement back analysis method". *Tunnelling and Underground Space Technology*, 38, 2013, pp.348-356.
9. Zhang Y., Xu W. Y., Shao J. F., Zhao H. B., Wang W., "Experimental investigation of creep behavior of clastic rock in Xiangjiaba Hydropower Project". *Water Science and Engineering*, 8(1), 2015, pp.55-62.
10. Kang J. H., Zhou F. B., Liu C., Liu Y. K., "A fractional non-linear creep model for coal considering damage effect and experimental validation". *International Journal of Non-Linear Mechanics*, 76, 2015, pp.20-28.
11. Wang G. B., Zhang L., Zhang Y. W., Ding G. S., "Experimental investigations of the creep-damage-rupture behaviour of rock salt". *International Journal of Rock Mechanics and Mining Sciences*, 66, 2014, pp.181-187.
12. Chen W., Konietzky H., "Simulation of heterogeneity, creep, damage and lifetime for loaded brittle rocks". *Tectonophysics*, 633, 2014, pp.164-175.
13. Erik E., "The Hoek–Brown Failure Criterion". *Rock Mechanics and Rock Engineering*, 45(6), 2012, pp.981-988.
14. Hoek E., Diederichs M.S., "Empirical estimation of rock mass modulus". *International Journal of Rock Mechanics and Mining Sciences*, 43(2), 2006, pp.203-215.
15. Fan W. H., "*Research of the Stability and Reliability of Surrounding Rocks in the Process of Gonghe Tunnel's Construction*". Master thesis of Chongqing University, China, 2009, pp.25-27.
16. Li Q. H., Chen M., Jin Y., Hou B., Zhang J., "Rock mechanical properties and brittleness evolution shale gas reservoir". *Petroleum Drilling Techniques*, 40(4), 2012, pp.17-22.
17. Shao B. P., Zhao Y. S., Wang Z. J., Zhao J. C., Wang Y., "Study of constitutive equation of granite rheological model with thermo-mechanical coupling effects". *Chinese Journal of Rock Mechanics and Engineering*, 28(5), 2009, pp.956-967.
18. Li W. G., Yang S. L., Xu J., Dong Q., "A new model for shale adsorptive gas amount under a certain geological conditions of temperature and pressure". *Natural Gas Geoscience*, 23(4), 2012, pp.791-796.
19. Wu S. Y., Zhao W., "Analysis of effective stress in adsorbed methane-coal system". *Chinese Journal of Rock Mechanics and Engineering*. 24(10), 2005, pp.1674-1678.
20. Deng Y. F., Liu S. Y., Zhang D. W., Xu H. B., "Comparison among some relationships between permeability and void ratio". *Northwestern Seismological Journal*, 33(s1), 2011, pp.64-66.